Nuclear Instruments and Methods in Physics Research B 326 (2014) 169–173

Contents lists available at ScienceDirect

Nuclear Instruments and Methods in Physics Research B

journal homepage: www.elsevier.com/locate/nimb

Defect accumulation in ThO_2 irradiated with swift heavy ions

Cameron L. Tracy [a], J. McLain Pray [b], Maik Lang [b], Dmitry Popov [c], Changyong Park [c], Christina Trautmann [d,e], Rodney C. Ewing [a,b,*]

[a] Department of Materials Science & Engineering, University of Michigan, Ann Arbor, MI 48109, USA
[b] Department of Earth and Environmental Sciences, University of Michigan, Ann Arbor, MI 48109, USA
[c] High Pressure Collaborative Access Team (HPCAT), Geophysical Laboratory, Carnegie Institution of Washington, Argonne, IL 60439, USA
[d] GSI Helmholtzzentrum für Schwerionenforschung, 64291 Darmstadt, Germany
[e] Technische Universität Darmstadt, 64287 Darmstadt, Germany

ARTICLE INFO

Article history:
Received 30 June 2013
Received in revised form 22 August 2013
Accepted 26 August 2013
Available online 28 January 2014

Keywords:
Ion irradiation
Actinides
Oxides
Diffraction
Spectroscopy

ABSTRACT

Polycrystalline ThO_2 was irradiated with 2.2 GeV Au ions and characterized by synchrotron X-ray diffraction, X-ray absorption spectroscopy, and Raman spectroscopy. The diffraction measurements indicated an increase in the unit cell parameter and the accumulation of heterogeneous microstrain with increasing ion fluence, both of which are consistent with a single-impact model of damage accumulation. An analytical fit of the data to a single-impact model yielded a saturation unit cell expansion of $0.049 \pm 0.002\%$ and a saturation strain of $10.4 \pm 0.2\%$. Cross-section data determined from the model values yielded effective ion track diameters of 1.9 ± 0.2 nm and 3.2 ± 0.3 nm for the two modifications, respectively, indicating that the tracks consist of a core region in which swelling and strain have occurred and a defect-rich halo in which microstrain is present but the initial unit cell parameter has not changed significantly. The spectroscopic analysis revealed the presence of significant local structural distortion in the irradiated material, but no evidence of systematic modification to the electronic state or chemical environment of the cations. This indicates that swift heavy ion irradiation of ThO_2 primarily produces simple point defects or defect agglomerates.

1. Introduction

ThO_2 exhibits the fluorite crystal structure ($Fm\bar{3}m$) and has applications as a nuclear fuel material, either alone or in a ThO_2–UO_2 mixture, with safety and waste management advantages over conventional UO_2 fuels [1,2]. However, its response to radiation damage, an important property for a nuclear fuel, is poorly characterized. Few radiation damage studies of this material have been performed and much of the available data is of a qualitative nature [3–5]. This is in contrast to related lanthanide and actinide oxides, such as CeO_2 and UO_2, for which a great deal of systematic irradiation data are available [6–8]. Quantitative, systematic investigation of radiation damage in ThO_2 is necessary in order to assess its performance as a nuclear fuel and to provide insight into the fundamental processes that govern the radiation response of fluorite-structured oxides.

Irradiation of insulators with swift heavy ions, which have energies greater than approximately 1 MeV per nucleon and deposit energy in a target material primarily through electronic energy loss (dE/dx), provides an appropriate simulation of fission fragment damage in nuclear fuels. Fission fragments are heavy atomic species with specific energies similar to those of swift heavy ions and for which electronic energy loss is the dominant stopping mechanism. The electronic excitation of the target material resulting from swift heavy ion irradiation can induce complex modifications to the atomic and electronic structures of the material which are often distinct from those induced by irradiation in the nuclear energy loss regime [9]. These modifications are generally attributed to either the production of Frenkel pairs during the decay of irradiation-produced self-trapped excitons [10] or to intense heating of a nanometric ionized region caused by electron–phonon coupling [11]. Previous investigation of ThO_2 [12] shows that it may exhibit self-trapped excitons, making this a possible mechanism for irradiation-induced damage creation in this material. Both effects are generally localized to an ion track, a cylindrical region along the trajectory of an impinging ion. By probing the crystallographic and electronic structures of an insulating material over a range of ion fluences, insight into the radiation response and the mechanisms by which defects accumulate in individual ion tracks can be obtained. This paper examines the damage produced by swift heavy ion irradiation of ThO_2 and, using synergistic diffraction and spectroscopic techniques, investigates the character and distribution of the resulting defects.

---

* Corresponding author at: Department of Materials Science & Engineering, University of Michigan, Ann Arbor, MI 48109, USA.
E-mail address: rodewing@umich.edu (R.C. Ewing).

0168-583X/$ - see front matter © 2014 Elsevier B.V. All rights reserved.
http://dx.doi.org/10.1016/j.nimb.2013.08.070

2. Experimental procedure

Polycrystalline ThO_2 was prepared by pressing powder, exhibiting crystallite sizes on the order of 1 μm, into 200 μm diameter holes drilled in 50 μm thick stainless steel sheets. Compact densities are typically lower than 60% theoretical density [13]. Irradiation of these samples was performed at beamline X0 of the UNILAC linear accelerator at the GSI Helmholtzzentrum für Schwerionenforschung in Darmstadt, Germany using 2.2 GeV ^{197}Au ions. The irradiation was carried out at room temperature and under vacuum to fluences of up to 5×10^{13} cm^{-2}, with the ion flux limited to $\sim 10^{9}$ cm^{-2} s^{-1} to avoid heating of the samples. The thickness of the samples, assuming 60% theoretical density, is less than the projected ion range obtained from calculations using the code SRIM-2008 [14] of 70.7 μm, indicating that all incident ions passed completely through the targets with a relatively constant electronic energy loss of 31.8 ± 1.7 keV/nm. The calculated nuclear energy loss is, for the entire ion path, always at least two orders of magnitude less than the electronic energy loss and is assumed to be negligible.

Modifications to the crystallographic and electronic structure of the irradiated samples were investigated by means of synchrotron X-ray diffraction (XRD), synchrotron X-ray absorption spectroscopy (XAS), and Raman spectroscopy. Angle dispersive XRD was performed at beam line HPCAT 16BM-D of the Advanced Photon Source at Argonne National Laboratory. A monochromatic beam of 25 keV ($\lambda = 0.4959$ Å), selected using a Si (1 1 1) double crystal monochromator with a focused spot size of 12 μm (v) × 5 μm (h) in the full width at half maximum, was used in transmission geometry and diffraction rings were recorded with a Mar345 image plate detector. Integrated two-dimensional patterns were produced with the software Fit 2d [15]. A collection time of 300 s was used for all diffraction patterns, which were fit with Pseudo-Voigt peaks to obtain individual peak widths. Unit cell parameters were determined by Rietveld refinement [16]. XAS at the Th L_{III}-edge was measured semi-simultaneously, immediately after the diffraction measurement without changing the beam spot on the sample. HPCAT 16BM-D's fixed-exit beam monochromator (Si (1 1 1) double crystals in pseudo channel cut mode) and switchable diffraction–absorption setup allowed consistent measurement of the two properties at an identical sample condition. Raman spectra were recorded in backscattering geometry on a Horiba Jobin Yvon (HR800) micro-Raman spectrometer with a 20 mW HeNe laser excitation source ($\lambda = 632.82$ nm), using a collection time of 10 s. Further details of the sample preparation, irradiation, and characterization are given elsewhere [17].

3. Results and discussion

Three modifications to the ThO_2 XRD patterns (Fig. 1) were observed following irradiation: shifts of all fluorite-structure diffraction maxima to lower 2θ values, peak broadening, and a reduction in the intensity of the diffraction maxima. No additional peaks were observed at any fluence, confirming that the fluorite structure is maintained under irradiation and further illustrating the exceptional stability of ThO_2 and similar fluorite-structured oxides under irradiation [17]. Additionally, no evidence of amorphization, in the form of broad, low-intensity X-ray scattering, was evident. This is in contrast to many oxide materials that exhibit phase transformations, amorphization, or both under swift heavy ion irradiation [18]. The peak shifts indicate an increase in the average unit cell parameter, while the intensity reduction suggests a decrease in the number of scattering atoms occupying the ideal fluorite structure atomic positions, resulting in a partial loss of coherent Bragg X-ray scattering. Both effects are attributed to irradiation-induced defect accumulation and the accompanying structural distortions over long- and short-range length scales, respectively [18]. In order to ascertain the source of the observed diffraction peak broadening, Williamson–Hall plots [19], as shown in Fig. 2(a) for Lorentzian peak shapes, were constructed from the XRD patterns obtained at each irradiation fluence. In this XRD analysis technique, the dependence of the peak broadening of individual diffraction maxima on the diffraction angle is studied. The $\tan(\theta)$ dependence of strain-induced peak broadening is distinguished from the $\cos^{-1}(\theta)$ dependence of crystallite size-induced peak broadening. By plotting $\sin(\theta)$, for each peak against $\beta\cos(\theta)$, where β is the induced peak broadening, a line is produced for which the slope depends on the material's microstrain and the y-intercept is inversely proportional to its grain size. This analysis showed that the irradiation-induced peak broadening in ThO_2 is due primarily to the accumulation of localized, heterogeneous strain with increasing ion fluence. No systematic change in the measured grain size, shown by the y-intercepts in Fig. 2(a), is evident. Such local strain in non-amorphized irradiated materials is commonly attributed to structural distortions near point defects or defect clusters [20].

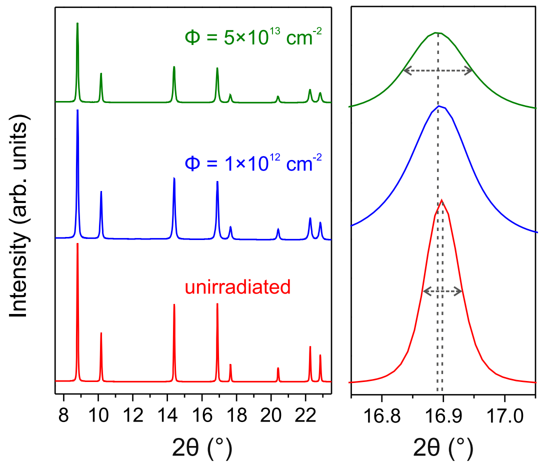

Fig. 1. Representative XRD patterns of irradiated and unirradiated ThO_2. Peak shifts to lower 2θ values, peak broadening, and a decrease in the intensity of all peaks occur with increasing ion fluence. The dotted lines show both the peak shifts, indicating an increase in unit cell parameter, and broadening, indicating the accumulation of heterogeneous strain.

Williamson–Hall analysis of the diffraction peak widths facilitated the extraction of average microstrain values as a function of fluence (Fig. 2(b)), while refinement of the peak shifts yielded the evolution of the material's unit cell parameter as a function of fluence (Fig. 2(c)). Both show an initial period of linear increase followed by saturation, indicating a single-impact mechanism for damage accumulation [21] in which the first ion to traverse a certain volume of the material fully modifies that region and subsequent ion impacts or track overlaps yield no further crystallographic alterations. As such, the data for both strain and unit cell parameters were fit with a single-impact model following the equation:

$$A = (A)_{sat}\left(1 - e^{-\Phi\sigma}\right) \tag{1}$$

where A is the change in the parameter being modified, in this case $\Delta a/a_0$ and ε, $(A)_{sat}$ is the saturation value of the parameter, Φ is the irradiation fluence, and σ is the ion track cross-sectional area, defining an ion track as the region in which the modification of interest occurs. This fitting procedure gives a maximum strain value of 10.4 ± 0.2% and a maximum unit cell parameter increase of 0.049 ± 0.002%. The latter unit cell swelling value is approximately one order of magnitude less than those obtained by Weber [6] for

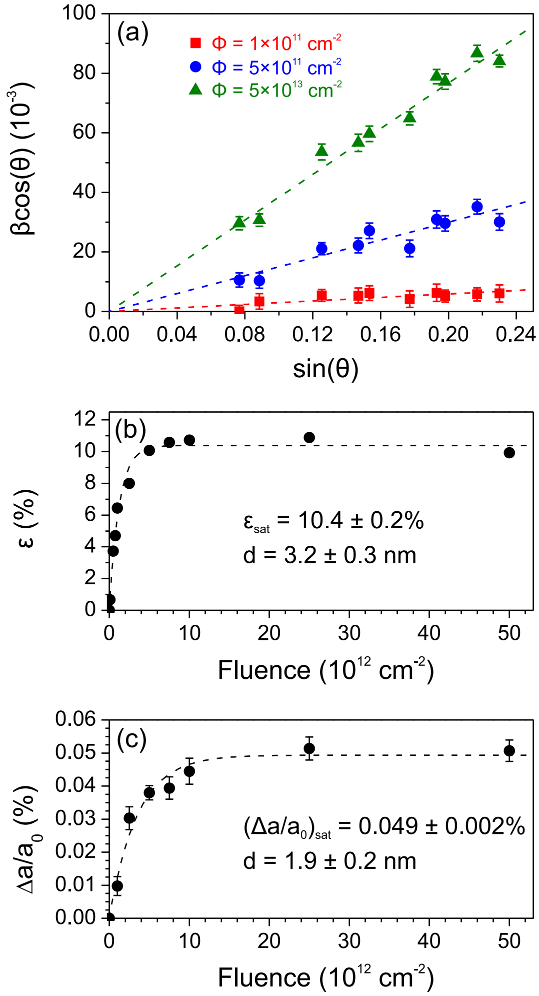

Fig. 2. (a) Williamson–Hall plots of representative XRD data collected from irradiated ThO_2. Straight lines were fit to the peaks for each fluence such that their slopes are proportional to the amount of heterogeneous strain present, while their *y*-intercepts are inversely proportional to the average grain size. Little change in grain size is evident, but there are significant increases in strain with increasing fluence. This indicates that the XRD peak broadening is primarily due to strain, rather than a reduction in grain size. (b) Heterogeneous strain, determined using Williamson–Hall plots, as a function of fluence. A single-impact model, Eq. (1), is fit to the data, yielding values for the strain at saturation and the diameter of the ion track in which this strain occurs. (c) Changes in the unit cell parameter of ThO_2 as a function of fluence. A single-impact model, Eq. (1), is fit to the data, yielding values for the swelling at saturation and the diameter of the ion track in which this swelling occurs.

alpha-particle irradiations of the similar fluorite materials CeO_2, UO_2, and PuO_2, suggesting that damage production by swift heavy ions in fluorite oxides is much less efficient than that of alpha-particle irradiation, which includes a significant nuclear energy loss component. It is, however, similar to the swelling of 0.06% observed by Ohno et. al. in fluorite CeO_2 irradiated with swift heavy ions [22]. Assuming cylindrical ion tracks, effective track diameters of 3.2 ± 0.3 nm and 1.9 ± 0.2 nm are determined for strain and unit cell expansion, respectively. The single-impact behavior of the microstrain accumulation differs from the linear behavior seen in Williamson–Hall analysis of oxides that are amorphized by swift heavy ions [23], suggesting a different mechanism, defect production, is responsible for this irradiation effect.

While the abovementioned benchmarks of swift heavy ion irradiation damage are useful for the quantification of the radiation tolerance of ThO_2, study of the defects produced in this material is necessary in order to fully understand its radiation response. To this end, spectroscopy techniques can provide valuable information regarding short length-scale atomic configurations. Raman spectroscopy of the unirradiated material (Fig. 3) shows only a single vibrational mode at approximately 465 cm^{-1}, in agreement with previous measurements [24]. This band is attributed to the triply degenerate T_{2g} vibration. Its intensity is significantly reduced with increasing ion fluence, indicating a breakdown of the selection rules accompanying the displacement of atoms from their equilibrium lattice sites and heterogeneous microstrain caused by defect production. The only other observed modification to the spectra is the growth of a broad band or of multiple overlapping bands in the range ~500–660 cm^{-1}. Guimbretière et. al. [25] observed similar Raman signals in approximately this range for fluorite-structured UO_2 irradiated with 25 MeV He ions, for which, as with the ions used in this study, the energy loss is primarily electronic. They differentiate the region into three distinct peaks at ~530, ~575, and ~ 635 cm^{-1} and attribute the low and high wavenumber peaks to hypo- and hyper-stoichiometric regions, respectively, and the middle peak to the Raman-forbidden LO mode [26]. This latter optical phonon mode has previously been observed in UO_2 irradiated with 200 keV Kr ions and has been shown to indicate a breakdown in the selection rules of fluorite materials due to structural damage accompanying irradiation-induced defect production [27]. Therefore, the appearance of a broad band in the Raman spectra of irradiated ThO_2 centered around 575 cm^{-1} and the reduction in the intensity of the T_{2g} mode both confirm the accumulation of structural distortion, or microstrain, with increasing fluence, resulting from the production of point defects or defect agglomerates.

In contrast to other f-block oxides, which are easily oxidized or reduced, thorium oxide is likely stable only as a dioxide. Very few trivalent thorium materials have been observed [28], none of which are oxides, and the element lacks pentavalent or higher oxidation states. Because oxidation and reduction from the Th^{4+} valence state are thus precluded, extended non-stoichiometric regions are not expected to form under irradiation. Cuboctahedral arrangements of anion defects, as are commonly observed in non-stoichiometric UO_2 [29], and similar charge-modified defect clusters were proposed by Guimbretière et. al. for the new low and high wavenumber bands, but are unlikely to occur in ThO_2. Instead,

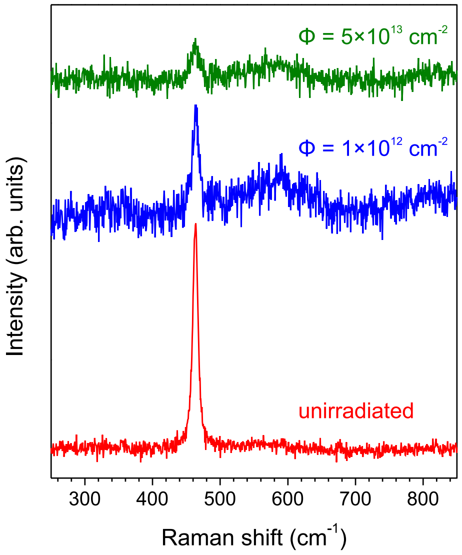

Fig. 3. Raman spectra of irradiated and unirradiated ThO_2. A pronounced decrease in the intensity of the T_{2g} mode at approximately 465 cm^{-1} is observed with increasing fluence, indicating the presence of structural distortion resulting from defect accumulation.

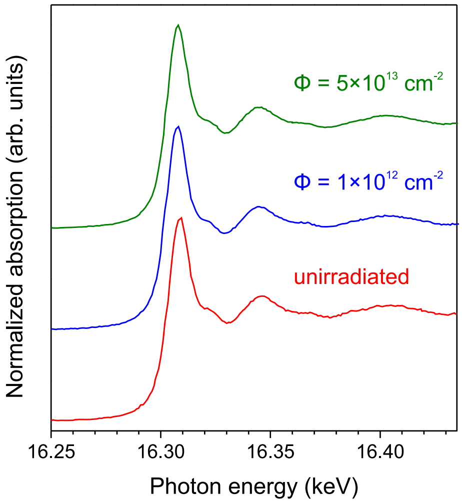

Fig. 4. XAS spectra of the Th L_{III}-edge of irradiated and unirradiated ThO_2. No change in the shape or position of the absorption edge is observed, suggesting that the electronic structure of ThO_2 is not significantly modified by swift heavy ion irradiation.

smaller regions of localized non-stoichiometry (e.g. hypo-stoichiometry around anion vacancies and hyper-stoichiometry around anion interstitials) might occur around defects, giving rise to the radiation-induced Raman modes at approximately 530 and 635 cm^{-1}. However, the weak Raman signal obtained from the irradiated samples precludes detailed analysis of the band or bands in this region. At the highest fluence achieved, 5×10^{13} cm^{-2}, the broad signal in the ~500–660 cm^{-1} region appears to decrease in intensity along with the T_{2g} mode, suggesting that a threshold degree of lattice distortion may exist above which these potential selection rule breakdown- and non-stoichiometry-induced modes are suppressed. Despite uncertainty in the attribution of the observed peaks, the T_{2g} mode decrease apparent in the Raman spectra of swift heavy ion irradiated ThO_2 shows strong agreement with the XRD results, confirming the production of extensive structural distortion, or heterogeneous strain, due to irradiation-induced defect formation.

The XAS results (Fig. 4) confirm that no systematic change in the electronic structure of the material or in the local bonding environment of the Th cations occurs after ion irradiation. This technique is sensitive to the valence state of the cation and its electronic configuration. The lack of modification to the Th L_{III}-edge in the form of either an energy shift or a change in the edge shape indicates that its chemical state is maintained despite the production of defects. This would not be the case if large concentrations of complex charge-coupled defect clusters, such as cuboctahedral anion interstitial complexes, were to form, as this would require a modification of the Th charge state in the non-stoichiometric region in order to maintain charge neutrality. Therefore, we propose that any modification to the electronic structure that results from changes in the local environment of the cations, as might occur by the production of Frenkel defects, is accommodated by long-range ionic interactions, rather than by short-range phase or chemical changes. The complementary Raman and X-ray spectroscopy results suggests that only simple point defects or defect aggregates, such as dislocation loops, are formed by swift heavy ion irradiation of ThO_2. Similar damage consisting of isolated and aggregated Frenkel pairs has been identified in non-amorphizable alkali halide ionic crystals due to swift heavy ion irradiation [10].

The difference in the ion track radius as determined from strain measurements compared with that determined from unit cell parameter measurements indicates a core–shell track morphology. Schwartz et al. [10] attribute similar core–shell morphology in fluorite-structured alkali halides to a central track region containing defect aggregates surrounded by a halo of isolated point defects. Thus, we conclude that, for ThO_2, the irradiation-induced strain measured by XRD and suggested by the observed breakdown of the Raman selection rules is due to the formation of Frenkel pairs and possibly defect agglomerates in the track cores. The measured increase in unit cell parameter as a function of fluence arises from swelling due to the presence of a certain saturation defect concentration, possibly accompanied by defect agglomeration, which, as per the single impact model, is achieved in an ion track after the first ion impact. The core is fully modified, such that a saturation defect concentration is achieved and a larger unit cell parameter is exhibited, while the shell is defect rich, such that heterogeneous strain occurs there, but does not contain a sufficient defect concentration or the required extent of defect agglomeration to exhibit an increase in the average unit cell parameter. Instead, only local atomic distance fluctuations due to compressive and tensile strains around interstitials and vacancies, respectively, are present. For this track morphology, microstrain, which is produced in both the core and shell track regions, accumulates more rapidly with ion fluence than swelling, which only occurs to a large extent in the track core. It is unlikely that distinct interfaces between the two regions are present, so the measured track radii should instead be taken as approximate values corresponding to a gradual decrease in defect concentration in the radial track direction. Core–shell track morphologies, in which a highly defective core is surrounded by a shell having a lower defect concentration, have also been posited by Lang et. al. [30] to occur in fluorite-derivative pyrochlore-structured complex oxides. In some such materials, swift heavy ion irradiation produces an amorphous track core surrounded by a fluorite-structured, antisite defect-rich shell and a pyrochlore-structured point defect-rich halo. While, in the case of pyrochlore, phase transformations accompany track formation, this result is consistent with those presented here in that concentric track regions are evident with decreasing defect concentration in the radial track direction, assuming the amorphous regions of the pyrochlores to be highly defective.

4. Conclusions

Irradiation of ThO_2 with swift heavy ions causes point defect formation through a single-impact mechanism. Spectroscopic analysis showed no evidence of complex defect clusters or of any change in the cation valence state. An increase in the unit cell parameter of the material and the accumulation of heterogeneous strain are exhibited with increasing ion fluence, both of which are attributed to structural distortion by the accumulated defects. The cross-sectional area per ion impact in which swelling occurs is smaller than that for which microstrain is present, indicating that the ion tracks consist of a central core region in which the average unit cell parameter has increased, due to the presence of a saturation defect concentration and possibly defect agglomerates, surrounded by a point defect-rich halo in which the average unit cell parameter change is small despite the presence of significant heterogeneous strain.

Acknowledgements

This work was supported by the Energy Frontier Research Center Materials Science of Actinides funded by the US Department of Energy, Office of Science, Office of Basic Energy Sciences (DE-SC0001089). Portions of this work were performed at HPCAT (Sector 16), Advanced Photon Source (APS), Argonne National Laboratory. HPCAT operations are supported by DOE-NNSA under

Award No. DE-NA0001974 and DOE-BES under Award No. DE-FG02-99ER45775, with partial instrumentation funding by NSF. APS is supported by DOE-BES, under Contract No. DE-AC02-06CH11357. The authors are grateful to Marcel Toulemonde for useful discussions.

References

[1] C. Lombardi, L. Luzzi, E. Padovani, F. Vettraino, Prog. Nucl. Energy 50 (2008) 944.
[2] K. Anantharaman, V. Shivakumar, D. Saha, J. Nucl. Mater. 383 (2008) 119.
[3] D.L. Douglass, S.E. Bronisz, J. Am. Ceram. Soc. 54 (1964) 158.
[4] J.H. Chute, J. Nucl. Mater. 21 (1967) 77.
[5] F.W. Clinard, D.L. Douglass, C.C. Land, J. Am. Ceram. Soc. 54 (1971) 177.
[6] W.J. Weber, Radiat. Eff. 83 (1984) 145.
[7] T. Wiss, H. Matzke, C. Trautmann, M. Toulemonde, S. Klaumünzer, Nucl. Instr. Meth. B 122 (1997) 583.
[8] B. Ye, A. Oaks, M. Kirk, D. Yun, W. Chen, B. Holtzman, J.F. Stubbins, J. Nucl. Mater. 441 (2013) 525.
[9] N. Itoh, D.M. Duffy, S. Khakshouri, A.M. Stoneham, J. Phys. Condens. Matter 21 (2009) 474205.
[10] K. Schwartz, C. Trautmann, R. Neumann, Nucl. Instr. Meth. B 209 (2003) 73.
[11] M. Toulemonde, Appl. Radiat. Isot. 46 (1995) 375.
[12] E.T. Rodine, P.L. Land, Phys. Rev. B 4 (1971) 2701.
[13] E. Luther, C. Necker, B. Mihaila, P. Papin, D. Guidry, T. Am, Nucl. Soc. 104 (2011) 257.
[14] J.F. Ziegler, M.D. Ziegler, J.P. Biersack, Nucl. Instr. Meth. B 268 (2010) 1818.
[15] A.P. Hammersley, ESRF Internal Report, ESRF97HA02T, "FIT2D: An Introduction and Overview" (1997).
[16] H.M. Rietveld, J. Appl. Crystallogr. 2 (1969) 65.
[17] M. Lang, F. Zhang, J. Zhang, C. Tracy, J.V. Ehr, Z.Q. Chen, C. Trautmann, R.C. Ewing, Nucl. Instr. Meth. B, accepted for publication.
[18] K.E. Sickafus, L. Minervini, R.W. Grimes, J.A. Valdez, M. Ishimaru, F. Li, K.J. McClellan, T. Hartmann, Science 289 (2000) 748.
[19] C.L. Tracy, M. Lang, J. Zhang, F. Zhang, Z. Wang, R.C. Ewing, Acta Mater. 60 (2012) 4477.
[20] G.K. Williamson, W.H. Hall, Acta Metall. 1 (1953) 22.
[21] C.J. Howard, T.M. Sabine, J. Phys. C Solid State 7 (1974) 3453.
[22] W.J. Weber, Nucl. Instr. Meth. B 166 (2000) 98.
[23] H. Ohno, A. Iwase, D. Matsumura, Y. Nishihata, J. Mizuki, N. Ishikawa, Y. Baba, N. Hirao, T. Sonoda, M. Kinoshita, Nucl. Instr. Meth. B 266 (2008) 3013.
[24] M. Lang, F. Zhang, W. Li, D. Severin, M. Bender, S. Klaumünzer, C. Trautmann, R.C. Ewing, Nucl. Instr. Meth. B 286 (2012) 271.
[25] V.G. Keramidas, W.B. White, J. Chem. Phys. 59 (1973) 1561.
[26] G. Guimbretière, L. Desgranges, A. Canizarès, G. Carlot, R. Caraballo, C. Jégou, F. Duval, N. Raimboux, M.R. Ammar, P. Simon, Appl. Phys. Lett. 100 (2012) 251914.
[27] T. Livneh, E. Sterer, Phys. Rev. B 73 (2006) 085118.
[28] P.R. Graves, Appl. Spectrosc. 44 (1990) 1665.
[29] J.R. Walensky, R.L. Martin, J.W. Ziller, W.J. Evans, Inorg. Chem. 49 (2010) 10007.
[30] A.D. Murray, B.T.M. Willis, J. Solid State Chem. 57 (1990) 52.
[31] M. Lang, J. Lian, J. Zhang, F. Zhang, W.J. Weber, C. Trautmann, R.C. Ewing, Phys. Rev. B 79 (2009) 224105.